ACS APPLIED MATERIALS & INTERFACES

Research Article

Cite This: ACS Appl. Mater. Interfaces 2019, 11, 38689−38696

www.acsami.org

Adsorption and Thermal Decomposition of Electrolytes on Nanometer Magnesium Oxide: An in Situ ^{13}C MAS NMR Study

Jian Zhi Hu,*[,‡] Nicholas R. Jaegers,[‡] Ying Chen, Kee Sung Han, Hui Wang, Vijayakumar Murugesan, and Karl T. Mueller*

The Joint Center for Energy Storage Research (JCESR), Pacific Northwest National Laboratory, Richland, Washington 99352, United States

Supporting Information

ABSTRACT: Mg batteries have been proposed as potential alternatives to lithium-ion batteries because of their lower cost, higher safety, and enhanced charge density. However, the Mg metal readily oxidizes when exposed to an oxidizer to form a thin MgO passivation surface layer that blocks the transport of Mg^{2+} across the solid electrode−electrolyte interface (SEI). In this work, the adsorption and thermal decomposition of diglyme (G2) and electrolytes containing $Mg(TFSI)_2$ in G2 on 10 nm-sized MgO particles are evaluated by a combination of in situ ^{13}C single-pulse, surface-sensitive $^{1}H-^{13}C$ cross-polarization (CP) magic-angle spinning (MAS) nuclear magnetic resonance, and quantum chemistry calculations. At 180 °C, neat G2 decomposes on MgO to form surface-adsorbed $-OCH_3$ groups that are captured as a distinctive peak located at about 50 ppm in the CP/MAS spectrum. At low $Mg(TFSI)_2$ salt concentration, the main solvation structure in this electrolyte is solvent-separated ion pairs without extensive Mg−TFSI contact ion pairs. G2, likely including a small amount of G2-solvated Mg^{2+}, adsorbs onto the MgO surface. At high $Mg(TFSI)_2$ salt concentrations, contact ion pairs between Mg and TFSI are formed extensively in the solution with the first solvation shell containing one pair of Mg−TFSI and two G2 molecules and the second solvation shell containing up to six G2 molecules, namely, $MgTFSI(G2)_2(G2)_6^+$. In the presence of MgO, $MgTFSI(G2)_2(G2)_6^+$ adsorbs onto the MgO surface. At 180 °C, the MgO surface stimulates a desolvation process converting $MgTFSI(G2)_2(G2)_6^+$ to $MgTFSI(G2)_2^+$ and releasing G2 molecules from the second solvation shell of the $MgTFSI(G2)_2(G2)_6^+$ cluster into the solution. $MgTFSI(G2)_2^+$ and $MgTFSI(G2)_2(G2)_6^+$ tightly adsorb onto the MgO surface and are observed by $^{1}H-^{13}C$ CP/MAS experiments. The results contained herein show that electrolyte composition has a directing role in the species present on the electrode surface, which has implications on the structures and constituents of the solid−electrolyte interface on working electrodes and can be used to better understand its formation and the failure modes of batteries.

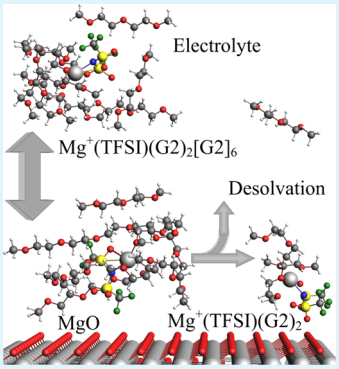

KEYWORDS: *magnesium battery, electrolytes, diglyme, $Mg(TFSI)_2$, ^{13}C NMR, and DFT NMR calculations*

INTRODUCTION

Energy storage represents an important technological field for continued global economic advancement. Batteries have long represented a convenient method for chemically storing energy, but rapidly increasing energy storage needs have driven extensive efforts to improve these materials in size, capacity, service life, and reusability. Rechargeable batteries such as Li-ion batteries have become a prominent power source for portable electronic devices and electric vehicles.[1,2] However, the demand for improved performance has prompted investigations into other multivalent cation systems. Mg metal batteries constitute an attractive alternative to Li-ion technology due to Mg's marked potential energy density enhancement over the Li-ion (3,833 vs 800 mA h/cc).[3] As such, extensive efforts have been made to better understand the interactions between the electrode surfaces and the electrolyte to drive the design of new materials with improved capacity and stability.[4] Repeated cycling introduces microstructure formation at the interface between the solid electrode and electrolyte due to migration of ionic species. This process often results in battery failure, highlighting the importance of identifying the interactions between the electrode surface and electrolyte to provide key understanding into the failure modes of Mg battery systems, which may be used in the rational design of improved systems.

The true surface of Mg battery electrodes is complex in nature due to Mg−metal interactions with electrolytes and air, where reported evidence has shown that MgO is a major constitute in the SEI of the Mg−metal anode in a magnesium battery system containing $Mg(TFSI)_2$/glyme electrolytes.[5] This is because the Mg metal readily oxidizes when exposed to an oxidizer, such as air,[6] to form a thin MgO surface layer. The presence of an MgO surface phase inevitably impacts the electrode surface-solvent/electrolyte interactions, thus affecting the performance of a Mg battery. Further, the high-molecular adsorption capacity of MgO enables molecules such as H_2O or

Received: July 14, 2019
Accepted: September 10, 2019
Published: September 10, 2019

DOI: 10.1021/acsami.9b11888
ACS Appl. Mater. Interfaces 2019, 11, 38689−38696

CO_2 to readily adsorb on the MgO surface. These molecules may, in turn, block the adsorption sites, preventing electrolytes from accessing the surface.[7,8] Indeed, it has been shown that the method of preparation affects the adsorption of molecules, which can modulate the reactivity for a variety of substrates.[9] This strongly suggests that even in battery applications, the preparation of the cell may result in contrasting surface oxide layers, and thus, different performances.

Though the specific reactivity may differ, MgO surfaces exhibit dehydrogenation activity, whereby alcohols have been shown to decompose into stable surface conjugate base species (methoxide, ethoxide, etc.) and carbonates, which may undergo further reactions with extended phase molecules or dehydrate in the absence of additional substrate interaction.[10−12] MgO is also effective at breaking C−O bonds, such as those of methyl formate and dimethoxyethane (DME, glyme, or G1).[9,13] The interactions of G1 with the MgO surface have been studied recently using computational modeling[13] due to its use as a solvent in Mg battery electrolytes, such as with magnesium(II) bis(trifluoromethane sulfonyl)imide ($Mg(TFSI)_2$), an electrolyte that exhibits high resistivity toward oxidation, high conductivity, and compatibility with most cathode materials.[14] The most stable decomposition interaction of G1 with the MgO surface was predicted by density functional theory (DFT) to result in the cleavage of one C−O bond and the exchange of an H atom between two fragments to form methanol and methoxy ethane which proceed through a methoxy intermediate and remain adsorbed on the surface. The study found that G1 decomposition was kinetically hindered by the surface oxide overlayer.[13]

The thermochemical decomposition of solvent materials is an important consideration for battery performance. The electrochemical cycling of batteries results in elevated cell temperatures (potentially >60 °C during discharge and even much greater locally at the electrode surface)[15,16] which may induce electrolyte and/or solvent reactivity over the course of numerous charge−discharge cycles. Cycling at high external temperatures has been shown to reduce cell lifetime as well, providing further need to investigate such interactions under high thermal stress conditions.[17] In situ nuclear magnetic resonance (NMR) spectroscopy is a technique well suited for probing the interactions between the solid surface and electrolyte materials.[18,19] In this work, we employ NMR to study the solvent−surface interactions under in situ conditions of significantly elevated temperatures to simulate the adsorption and potential thermal decomposition of the solvent and electrolytes on the MgO surface. Specifically, we investigate electrolytes containing $Mg(TFSI)_2$ in diglyme (G2) because G2 is a commonly used solvent in Mg-battery applications due to its improved stripping kinetics of Mg^0 over glyme (G1 or DME).[6]

EXPERIMENTAL METHODS

Samples. Electrolytes of 0.1 M and 1.0 $Mg(TFSI)_2$ in G2 were prepared as follows in an argon-filled glovebox. A stoichiometric amount of $Mg(TFSI)_2$ (99.5%, Solvionic, France) was added to G2 (99.5%, Sigma-Aldrich) in a 5 mL volumetric flask under stirring at room temperature. $Mg(TFSI)_2$ was dried for two days under vacuum at 180 °C, and the G2 was dried over activated 3 Å molecular sieves until its moisture content was determined to be below 30 ppm by a Karl-Fisher titrator (Metrohm). Magnesium oxide nanopowder (MgO, 99.9%, 10 nm) was purchased from US Research Nanomaterials, Inc. with a size distribution of 5% <5 nm, 90% ∼10 nm, 5% >10 nm (with up to 1% as 30−40 nm) and a specific surface area of 85−120 m^2/g.

In Situ Natural Abundance MAS NMR Spectroscopy. In situ ^1H and ^{13}C single-pulse (SP) magic-angle spinning (MAS) NMR experiments with high power proton decoupling were performed on a Varian/Agilent Inova wide-bore 300 MHz NMR spectrometer using a 7.5 mm ceramic pencil-type MAS probe, operating at ^{13}C and ^1H larmor frequencies of 75.430 and 299.969 MHz, respectively. A custom-made 7.5 mm outside diameter all-zirconia MAS rotor that was capable of 100% fluid seal under the condition of a combined high-temperature and high-pressure operating environments[20] was employed for in situ MAS NMR investigations. ^{13}C spectra were referenced to tetramethylsilane (TMS at 0 ppm) using adamantane as a secondary reference, that is, with ^{13}C of CH_2 at 38.48 (downfield peak). All species, regardless of being adsorbed on the particle surface or in the bulk solution phase, are quantitatively detected by the SP experiment provided the recycle delay time (d_1) is larger than five times the relaxation time when a $\pi/2$ pulse is used. By using a smaller tip pulse angle less than $\pi/2$, a reduced recycle delay time can be used for quantitative measurement. To determine the recycle delay time, an array of d_1 times was collected with $\pi/4$ pulses and used to ensure d_1 was sufficiently long for quantitative measurement (e.g., 5 s).

$^1H-^{13}C$ cross-polarization (CP) MAS NMR was used to identify only those species that are adsorbed onto a solid surface because CP/MAS depend on static dipolar interaction between ^1H and ^{13}C spins. In bulk solutions, fast and random molecular motions reduce the time-averaged ^1H and ^{13}C dipolar interaction to zero, so the species in bulk solution are not detected in the CP experiment. In contrast, the interaction of molecules with a solid surface limits the motion of the adsorbed molecules to yield a nonzero time-averaged $^1H-^{13}C$ dipolar interaction that may be sufficiently strong for establishing an effective CP, making CP/MAS a surface-sensitive method. Because the efficiency of a CP experiment depends on many factors such as the strength of $^1H-^{13}C$ dipolar interaction and the ^1H spin-lattice relaxation in the rotation frame, $T_{1\rho}$, a CP experiment at a fixed contact time is generally not quantitative but is an excellent method for detecting surface species. A 0.5 s recycle delay time (d_1), contact time (ct) time of 2.6 ms, and a ^1H decoupling field strength of 62.5 kHz were employed to collect these spectra.

Methods for Loading Samples into a Sealed MAS NMR Rotor. Prior to ^{13}C SP or $^1H-^{13}C$ CP/MAS NMR experiments, the 10 nm MgO powder samples were pretreated in a quartz tube connected to a vacuum (10^{-3} Torr with 20% O_2) manifold controlled to low O_2 partial pressure and heated to either 200 or 550 °C for 10 h. The valve on the quartz tube was closed, and the samples were then allowed to cool prior to relocation to a dry nitrogen glovebox for packing. The valve was opened and a controlled quantity of MgO powder was packed into a sealed NMR rotor. Subsequently, a controlled amount of either G_2 or G_2 + $Mg(TFSI)_2$ was added to the rotor in the glovebox and quickly sealed. The seal of the rotor was confirmed by comparing the mass prior to and after the NMR measurements. In each case, identical masses were recorded, indicating a perfect seal of the MAS rotor during the measurements.

Quantum Chemistry Calculations. Computational modeling of the NMR chemical shifts was carried out using the Amsterdam Density Functional (ADF-2014) package.[21] Geometries were optimized using the generalized gradient approximation with Grimme's third generation dispersion correction[22] applied to the Becke−Lee−Yang−Parr[23,24] functional employed for geometry optimization. All calculations were carried out by using the all-electron TZ2P basis set (triple-ζ, 2-polarization function) with the Slater-type orbitals[25] implemented in the ADF program. ^{13}C NMR calculations were performed based on the geometry-optimized structures at the same level of the theory and with the same basis set to evaluate the chemical shielding for each atom. The calculated ^{13}C chemical shielding for adamantane is 136.08 ppm. To convert the calculated shielding to the experimentally observed scale with reference to adamantane (38.48 ppm), the following equation is used, that is, $\delta_{obs} = 136.08 - \delta_{calc} + 38.48$.

DOI: 10.1021/acsami.9b11888
ACS Appl. Mater. Interfaces 2019, 11, 38689−38696

RESULTS AND DISCUSSION

Reactivity of Solvent G2 on MgO Coated with Carbonates. A single and relatively broad peak centered at about 167.6 ppm with a half line width of 484 Hz (or 6.42 ppm) is observed in the $^{1}H-^{13}C$ CP/MAS NMR spectrum of the 10 nm MgO powder pretreated at a temperature of 200 °C (Figure 1a). This peak is attributed to surface carbonate

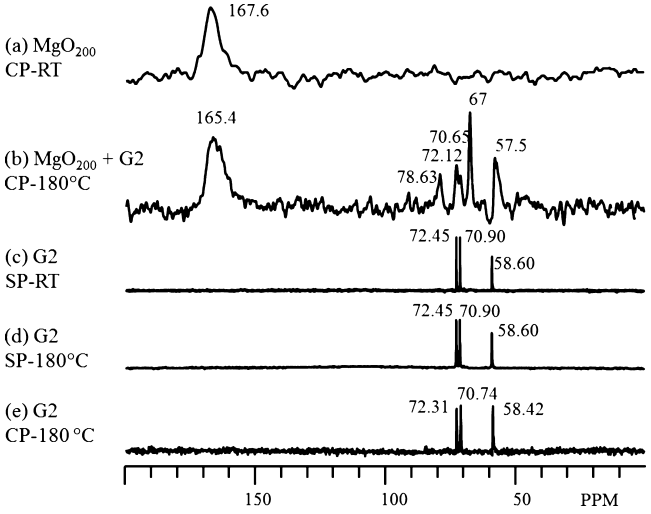

Figure 1. ^{13}C CP/MAS or SP/MAS spectra acquired at a sample spinning rate of about 3.5 kHz and at room temperature. (a) CP/MAS of pure 10 nm MgO immediately after pretreatment at 200 °C (MgO_{200}); this spectrum was acquired after the mixture was heated to 180 °C for 1 h; (a) was acquired with 97 872 scans; (b) CP/MAS of 2 μL G2 + 66.1 mg MgO_{200}. This spectrum was acquired with 100k scans; (c–e) samples comprised of 25 μL G2: (c) SP spectrum immediately taken after loading into the rotor; 128 scans were collected; (d) SP after heating to 180 °C for 1 h with 1748 scans; (e) CP spectrum with 99 052 scans.

(CO_3^{2-}),[26] including bicarbonate (HCO_3^-) and carbonate interacting with Mg, that is, $MgCO_3$.[27,28] These carbonate species likely originate from CO_2's interaction with the MgO surface during the commercial MgO manufacturing process (either from decomposition of surface formate species or from ambient air)[29] that cannot be removed at a pretreatment temperature of 200 °C. The reactivity of this MgO sample with G2 at a reaction temperature of 180 °C is shown in Figure 1b by the $^{1}H-^{13}C$ CP/MAS spectrum. In addition to the carbonate peak, there are at least five upfield peaks observed; c.a. 57.5, 67, 70.65, 72.12, and 78.63 ppm. All three ^{13}C peaks show a minor upfield shift of about 0.15 ppm when interacting with the material surface. Based on the pure G2 results, the peaks in Figure 1b can be assigned as the MgO surface adsorbed G2: CH_3 (57.5 ppm)–O–CH_2 (72.12 ppm)–CH_2 (70.65 ppm)–O–CH_2 (70.65 ppm)–CH_2 (72.12 ppm)–O–CH_3 (57.5 ppm), and the MgO surface-mediated decomposed products, or G2 interacting with surface carbonates, with peaks located at 78.63 and 67 ppm. Pure G2 inside the zirconia rotor shows no reactivity at 180 °C (Figure 1c,d), indicating that the stabilized bulk ZrO_2 crystal (rotor material) is inert to G2 under our reaction conditions. This is evident by comparing the ^{13}C SP spectra prior to and after treating at 180 °C for 1 h (Figure 1c,d). G2 does adsorb onto the inner surface of the rotor wall and the adsorbed G2 can be captured by ^{13}C CP/MAS (Figure 1e) despite the rather low surface area of the rotor, that is, $\pi \times 4.5$ mm $\times$ 15 mm = 212 mm^2.

Reactivity of Solvent G2 on MgO with Clean Surface. Pretreatment of the 10 nm MgO powder at a temperature of 550 °C and above effectively removes surface carbonates, generating a clean MgO surface, evidenced by the absence of the 167.7 ppm peak in Figure 2. To investigate the reactivity of

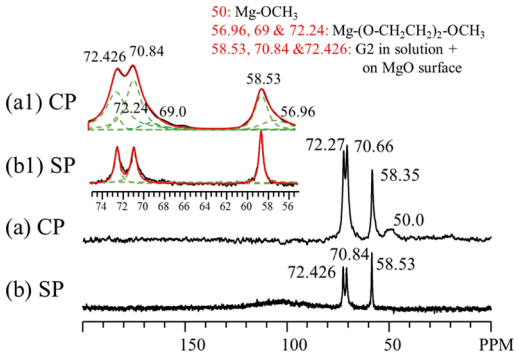

Figure 2. (a) ^{13}C CP/MAS and SP/MAS (b) spectra obtained on 115.7 mg MgO_{550} + 25 μL G2 after reacting at 180 °C for 1 h. (a1,b1) are horizontally expanded regions of (a,b) between 55 and 75 ppm. (a) was acquired with 77 400 scans; (b) was acquired with 2196 scans.

G2 with a clean MgO surface (MgO_{550}), MgO_{550} was mixed with G2 in a sealed all-zirconia MAS rotor for NMR measurements. After in situ heating at 180 °C for 1 h, ^{13}C SP and $^{1}H-^{13}C$ CP/MAS spectra were acquired. These results are presented in Figure 2. Surface methoxy species (later validated by DFT) in the form of Mg–OCH_3 are clearly observed in the $^{1}H-^{13}C$ CP/MAS spectrum (Figure 2a) with its unique peak centered at ~50 ppm. This forms from the cleavage of –OCH_3 in G2 ($CH_3O-CH_2CH_2-O-CH_2CH_2-OCH_3$) by MgO at 180 °C. The remaining G2 fragment interacts with the lattice oxygen of the MgO surface to form a $CH_3O-CH_2CH_2-O-CH_2CH_2-O-Mg$ structure. The decomposition process is depicted in Figure 3. Indeed, the ^{13}C CP/MAS spectrum between 55 and 75 ppm (Figure 2a1) cannot be fit by using only three peaks (58.53, 70.84, and

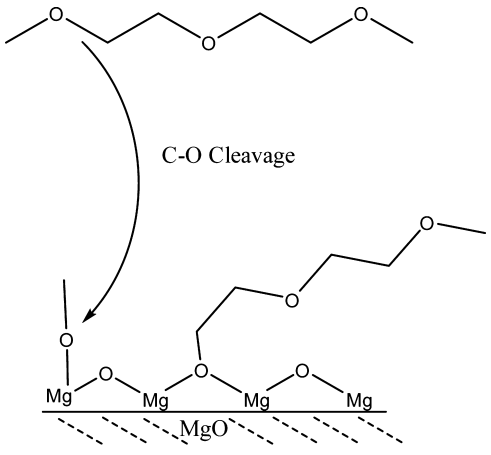

Figure 3. Schematic depiction of solvent G2 ($CH_3OCH_2CH_2OCH_2CH_2OCH_3$) decomposition on MgO to form CH_3OMg and $MgOCH_2CH_2OCH_2CH_2OCH_3$ via C–O cleavage of diglyme.

DOI: 10.1021/acsami.9b11888
ACS Appl. Mater. Interfaces 2019, 11, 38689–38696

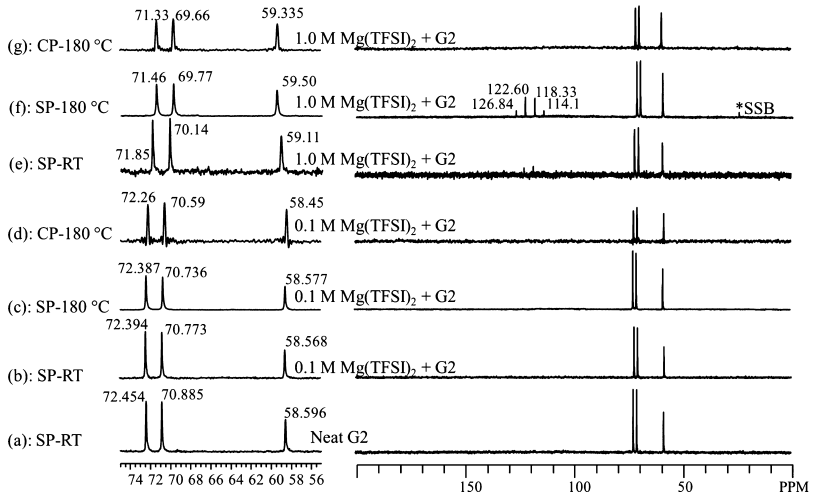

Figure 4. ^{13}C SP/MAS (a–c, e,f) and CP/MAS (d,g) spectra. (a) 25 μL pure G2; (b–d) 33.7 μL 0.1 M $Mg(TFSI)_2$ + G2; (e–g) 35 μL 1.0 M $Mg(TFSI)_2$ + G2. (a,b,e) prior to heat treatment; (c,f) after heat treatment. Number of scans are 128 (a), 70 (b), 4000 (c), 160 000 (d), 24 (e), 4000 (f), and 111 532 (g) scans, respectively. "*" SSB indicates the spinning sideband. The four peaks at 114.1, 118.33, 122.60, and 126.84 ppm are signals from TFSI–CF_3 carbon.

72.426 ppm) as those of the SP spectrum (Figure 2b1). Three additional peaks assigned to $CH_3O–CH_2CH_2–O–CH_2CH_2–O–Mg$ and located at approximately 56.96, 69, and 72.242 ppm are utilized to generate a good fit. The upfield shift relative to its corresponding SP $–OCH_3$ carbon spectral peak is justified by NMR computational modeling below. Note that the cleavage of $–OCH_3$ in DME (G1) has been previously suggested by computational modeling studies as a favorite mechanisms for DME decomposition on the Mg–metal surface.[13]

Adsorption of Electrolytes ($Mg(TFSI)_2$ + G2) on Clean Surface MgO. Two $Mg(TFSI)_2$ concentrations, that is, 0.1 and 1.0 M in G2, are examined for investigating electrolyte concentration-dependent adsorption and decomposition on a clean MgO surface. To investigate their reactivity with the inner wall of the zirconia rotor surface and the extent of Mg–TFSI contact ion formation, both ^{13}C SP and CP MAS NMR experiments were carried out first without using MgO_{550} for comparison to the spectra of neat G2. Clearly, no observable reaction between these two electrolytes and the rotor was observed based on the results presented in Figure 4, evident in the expanded spectral region from 55 to 75 ppm, where only three ^{13}C peaks corresponding to G2 are observed. For the 0.1 M $Mg(TFSI)_2$ + G2 sample, the chemical shifts of the three ^{13}C peaks for G2, 58.568, 70.771, and 72.394 ppm prior to Figure 4b and post heat treatment at 180 °C for 1 h (Figure 4c) are essentially identical and slightly shifted upfield by 0.03–0.1 ppm when compared to neat G2 (Figure 4a). In contrast, 1.0 M $Mg(TFSI)_2$ + G2 reveals an $–OCH_3$ peak that is downfield-shifted by about 1 to 59.50 ppm, while the two $–OCH_2CH_2O–$ peaks are upfield-shifted by approximately 1 to 69.77 and 71.46 ppm. It has been reported[4] that low salt concentrations (0.04 M) of $Mg(TFSI)_2$ in G2 result in nearly complete dissociation of Mg–TFSI, while contact ion pairs are observed at higher concentrations (0.4 M) with one $TFSI^-$ anion in the first solvation shell around Mg^{2+}. Therefore, in the 0.1 M $Mg(TFSI)_2$ + G2 sample, the majority of Mg–TFSI are dissociated by G2, while for the 1.0 M $Mg(TFSI)_2$ + G2 sample, the majority of Mg–TFSI forms contact ion pairs. The difference in the shifts of ^{13}C peaks for the G2 in the 0.1 and 1 M salt concentrations are, thus, a result of detailed solvation structural changes that is detailed by NMR computational modeling studies below.

Mixing MgO_{550} with 0.1 M $Mg(TFSI)_2$ in G2 reveals no evidence of electrolyte decomposition from the ^{13}C SP and CP/MAS spectra after thermal treatment at 180 °C for 1 h (Figure 5). However, adsorption of G2 onto the MgO surface

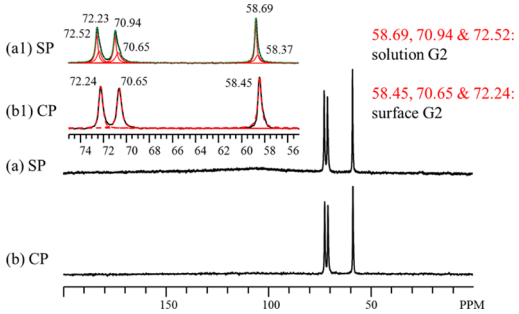

Figure 5. (a) ^{13}C SP/MAS (a) and CP/MAS (b) spectra obtained on 55.2 mg MgO_{550} (clean surface) + 34.5 mg 0.1 M $Mg(TFSI)_2$ in G2 after in situ heat treatment at 180 °C for 1 h. (a1,b1) are horizontally expanded regions of (a,b), highlighting MgO surface-adsorbed G2 with peaks located at approximately 58.4, 70.65, and 72.23 ppm. 4000 (a) and 97 126 (b) scans were employed. No electrolyte decomposition is observed for this sample.

is captured in both the SP (Figure 5a,a1) and the CP (Figure 5b,b1) experiments with the corresponding peaks located at approximately 58.4, 70.65, and 72.23 ppm. The other three peaks in the SP/MAS spectrum, 58.69, 70.94, and 72.52 ppm, from liquid phase G2 are not detected in the CP experiment due to fast random molecular motion. The relative abundance of these species may be quantified from SP spectral deconvolution (Supporting Information). The results indicate that about 63% of G2 is present in the solution phase, while the rest is surface-constrained. The $–CF_3$ carbons of TFSI are not detected in either the bulk solution phase or the MgO surface due to the low abundance and number of scans used. Nevertheless it is safe to say that the MgO surface contains a negligible amount of tightly bonded TFSI at a low salt concentration of 0.1 M.

DOI: 10.1021/acsami.9b11888
ACS Appl. Mater. Interfaces 2019, 11, 38689–38696

Significant changes are observed when the salt concentration is increased to 1.0 M. Figure 6 summarizes the ^{13}C SP/MAS and CP/MAS results obtained on a sample containing MgO_{550} and 1.0 M $Mg(TFSI)_2$ in G2 after in situ heat treatment at 180 °C for 1 h. SP/MAS detect all of the species regardless they are in the bulk solution or adsorbed onto the MgO surface. Six major peaks are found in the SP/MAS spectra (Figure 6a,a1) that are related to G2 and/or surface-adsorbed G2−Mg−TFSI complexes with peaks centered at about 59.5, 61.11, 69.0, 69.84, 70.81, and 71.6 ppm in addition to two minor shoulder peaks at 58.75 and 72.6 ppm. A set of relatively sharp solution $-CF_3$ carbons located at 113.89, 118.3, 122.58, and 127.1 ppm is also observed. The two minor shoulder peaks have ^{13}C chemical shifts similar to the major solution ^{13}C SP/MAS peak in Figure 5a1 for the 0.1 M $Mg(TFSI)_2$ in G2 and are thus readily assigned to G2 molecules in solution. This free solution G2 species accounts for approximately 7% of the observed G2 signals (Supporting Information). The CP/MAS spectra, which detects only those species that are tightly adsorbed onto the MgO surface, (Figure 6b,b1), clearly show that (i) the TFSI anion is adsorbed onto the MgO surface, evidenced by the relatively broad peaks located at about 118.3 and 122.4 ppm for TFSI; and (ii) G2 molecules are adsorbed onto the MgO surface with peaks at 59.28, 69.74, and 71.49 ppm. Given the similarities of the ^{13}C chemical shifts for the adsorbed G2 (Figure 6b1) and those in bulk solution (Figure 4e,f), the surface-adsorbed G2 and TFSI must also maintain contact ion pairs in the same way as pure electrolytes of 1.0 M $Mg(TFSI)_2$ in G2. Three new and symmetric peaks in the CP/MAS spectrum (Figure 6b1) are observed at 60.94, 68.85, and 70.63 ppm. Compared with their counterparts in the SP spectrum (Figure 6a1), these three peaks in the CP spectrum are sharper and upfield-shifted by about 0.2 ppm, a trend that is consistent with surface adsorption discussed throughout this work. Furthermore, these three peaks have shift trends, that is, with the $-OCH_3$ group shifted downfield and the two CH_2 groups shifted upfield, similar to 1.0 M electrolyte concentration versus neat G2 but with about 1.0 ppm more magnitude than the neat 1.0 M electrolytes. Given this trend, we hypothesize a different solvation structure of Mg−TFSI contact ion pair by G2 on the MgO surface rather than G2 decomposed products on the MgO surface. Quantum chemistry calculations are utilized to help identify the possible structures related to the 60.94, 68.85, and 70.63 ppm ^{13}C peaks.

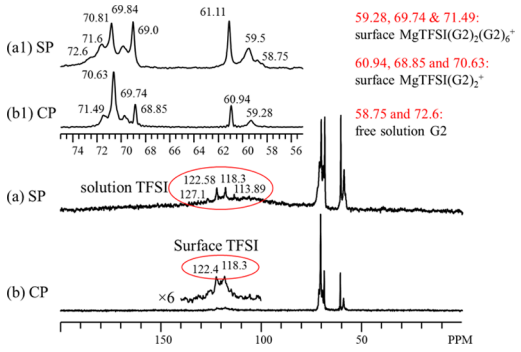

Figure 6. (a) ^{13}C SP/MAS (a) and CP/MAS (b) spectra obtained on 61.4 mg MgO_{550} (clean surface) + 36.5 mg 1.0 M $Mg(TFSI)_2$ in G2 after in situ heat treatment at 180 °C for 1 h. (a1,b1) are horizontally expanded regions of (a,b), highlighting MgO surface-mediated adsorption products with peaks at approximately 60.94, 68.85, and 70.63 ppm, surface adsorbed G2 with peaks located at approximately 59.28, 69.74, and 71.49 ppm, and surface adsorbed $TFSI^-$ at 118.3 and 122.4 ppm. Number of scans: 4000 (a) and 70 500 (b) scans, respectively. No electrolyte decomposition is observed for this sample.

Quantum Chemistry Calculations. *Validation of the Methoxy Groups on the MgO Surface.* It is observed (Figure 2) that the decomposition of G2 over the clean MgO surface produces a ^{13}C CP/MAS peak centered at about 50 ppm that is about 8.4 ppm upfield-shifted relative to the $-OCH_3$ carbon in neat G2 (Figure 4). Quantum chemistry predicts a 7.7 ppm upfield shift relative to that of neat G2 (Figure 7a) using a small cluster model consisting of 8 Mg + 8 O and a $-CH_3$ group interacting with one of the interior O-atoms (Figure 7b). The excellent agreement between theory and the experiment validates that the 50.0 ppm peak is indeed the $-OCH_3$ carbon from the decomposed G2. The decomposed $-OCH_3$ group occupying the MgO surface lattice defect site would fit the model as depicted in Figure 7. The remaining fragment of decomposed G2, that is, $CH_3-O-CH_2CH_2-OCH_2CH_2-$, would interact with the MgO surface via the surface MgO lattice oxygen site, but the model in Figure 7 is too small for accurate prediction.

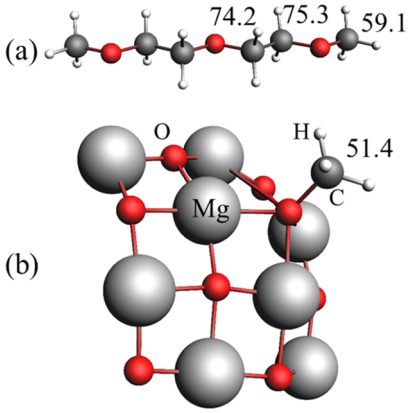

Figure 7. Models for quantum chemistry calculations of isotropic ^{13}C NMR chemical shielding. (a) Neat G2; (b) a $-OCH_3$ group on a model MgO surface carrying one positive charge simulating a surface defect site, that is, an oxygen vacancy. The numbers labeled by the carbons are calculated absolute shielding.

Solvation Structures in the Electrolytes. For 1.0 M $Mg(TFSI)_2$ in the G2 sample, there are, on average, 6.4−6.7 G2 molecules associated with one $Mg(TFSI)_2$. Contact ion pairs between the Mg^{2+} and $TFSI^-$ form with the first solvation shell containing two G2 and the second solvation shell containing up to six G2 molecules are reported previously.[4] Given fast molecular exchange among the various G2 molecules, that is, much faster than the NMR time scale of ms in liquid, an average ^{13}C chemical shift of each chemically equivalent carbon is observed experimentally for each carbon position in G2 and TFSI. The calculated averaged ^{13}C chemical shifts for the models containing one pair of Mg−TFSI and two G2 in the first shell with 5 or 6 G2 in the second shell are listed in Table 1, where the calculated shifts on an isolated G2 molecule (i.e., neat G2) are also included for comparison. For the model of $(MgTFSI(G2)_2(G2)_6^+)$, the results clearly show that the $-OCH_3$ carbon is downfield by about 0.83 ppm (higher ppm) relative to that of neat G2, while the two CH_2 carbons are upfield-shifted by about 1.2 and 0.63

DOI: 10.1021/acsami.9b11888
ACS Appl. Mater. Interfaces 2019, 11, 38689−38696

Table 1. Quantum Chemistry Predicted ^{13}C Isotropic Chemical Shifts on Various Models of Solvation Structures of $Mg(TFSI)_2$ in G2[a]

Structure	Label	CH_3	CH_2-Inner	CH_2-Outer
		Avg. ppm (1^{st})[b] [2^{nd}][c]	Avg. ppm (1^{st}) [2^{nd}]	Avg. ppm (1^{st}) [2^{nd}]
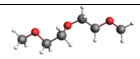	G2	59.07	74.15	75.27
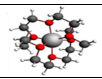	$Mg(G2)_2^{2+}$	61.71	73.14	74.11
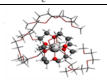	$Mg(G2)_2[G2]_6^{2+}$	61.12 (64.29) [60.07]	74.27 (72.88) [74.73]	75.21 (74.7) [75.38]
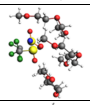	$TFSI(G2)_3^-$	58.9	75.2	76.8
	$MgTFSI(G2)_2^+$	60.83	69.83	73.30
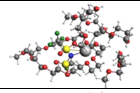	$MgTFSI(G2)_2[G2]_5^+$	60.8 (63.3) [59.8]	72.8 (70.9) [73.6]	75.1 (73.4) [75.7]
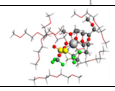	$MgTFSI(G2)_2[G2]_6^+$	59.9 (62.64) [58.99]	72.94 (71.31) [73.49]	74.64 (74.25) [74.77]
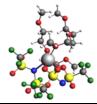	$MgTFSI_2(G2)_2$	59.1	76.4	75.7
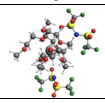	$MgTFSI_2(G2)_3$ From crystal	61.97	75.59	72.52

[a]The chemical shifts are referenced to adamantane at 38.48 ppm: $\delta_{obs} = 136.08 - \delta_{Calc} + 38.48$. [b]The average chemical shifts of each chemically equivalent carbon in the first solvation shell. [c]The average chemical shifts of each chemically equivalent carbon in the second solvation shell.

ppm (lower ppm) relative to those of neat G2, in excellent agreement with the experimental observations in Figure 4 (~1.0 ppm downfield shift for $-OCH_3$ and about 1.0 ppm for each of the two CH_2 carbons experimentally). For the 0.1 M $Mg(TFSI)_2$ in the G_2 sample, contact ion pairs (Mg−TFSI) should also form for part of Mg^{2+} as the experimental ^{13}C chemical shift trends of G2 (Figure 4) are similar to those of 1.0 M concentration, albeit the amount of shifts are much smaller (i.e., with 0.03 ppm downfield shift for $-OCH_3$, while about 0.11 and 0.06 ppm upfield-shifted for the CH_2 carbons). The smaller shifts may be explained by the fast chemical exchange between G2 in the solvation shells and those in the bulk solution because 90% of G2 are free. The existence of Mg^{2+} that are solvated only by G2 molecules for low $Mg(TFSI)_2$ concentration[4] is reported earlier that is validated by the calculated results on the model containing one Mg^{2+} solvated by 2 G2 in the first solvation shell and 5−6 G2 in the second shell (Table 1). The calculated chemical shifts for the CH_2 carbons (averaged between the first and the second shells) are almost the same to those of the neat G2 case, while the $-OCH_3$ carbons are shifted downfield, a trend still consistent with experimental results on 0.1 M $Mg(TFSI)_2$ in the G2 case. Given the large amount of free G2 in the 0.1 M sample, it is expected that most Mg^{2+} are solvated only by G2 without forming contact Mg−TFSI ion pairs, consistent with the results obtained on ^{25}Mg NMR and the related quantum chemistry studies earlier.[4]

Nature of Adsorbed Species on MgO from ^{13}C CP/MAS for 1.0 M $Mg(TFSI)_2$ in G2 (Figure 6b1). Relative to the solvation structure of $MgTFSI(G2)_2(G2)_6^+$, the solvation structure of $MgTFSI(G2)_2^+$ predicted by quantum chemistry shows a downfield shift of 0.93 ppm for the $-OCH_3$ carbon of G2 and upfield shifts of 3.1 and 1.3 ppm for the two kinds of CH_2 carbons. These shift trends (i.e., up- or downfield) are in excellent agreement with experimental results of downfield shift of 1.7 for $-OCH_3$, upfield shifts of 0.89 and 0.86 ppm for the two CH_2 groups. Thus, we can assign the 60.94, 68.85, and 70.63 ppm ^{13}C peaks in the CP/MAS spectrum of 1.0 M $Mg(TFSI)_2$ in G2 on MgO (Figure 6b1) to the solvated $MgTFSI(G2)_2^+$ clusters adsorbed on the MgO surface. It has been established above that the relatively broader peaks located at 59.28, 69.74, and 71.49 ppm in Figure 6b1 are from surface-adsorbed $MgTFSI(G2)_2(G2)_6^+$ that is also the main solvation species in the 1.0 M sample. Based on the results obtained from this work, the physical picture of adsorption at high salt concentration of $Mg(TFSI)_2$ in G2 (the 1 M case) becomes clear. The solvation structure in the electrolytes ($MgTFSI(G2)_2(G2)_6^+$) interacts with the MgO surface and is thus captured in the CP spectrum. The MgO surface stimulates a desolvation process converting $MgTFSI(G2)_2(G2)_6^+$ to $MgTFSI(G2)_2^+$ and frees the G2 molecules in the second solvation shell of the $MgTFSI(G2)_2(G2)_6^+$ cluster back into the electrolyte solution. This lowers the concentration of the salt in the electrolytes, where the excessive G2 are observed in the ^{13}C SP spectrum with characteristic peaks at 58.75 and 72.6 ppm.

CONCLUSIONS

The adsorption and thermal decomposition of diglyme (G2) and electrolytes containing $Mg(TFSI)_2$ in G2 on 10 nm-sized MgO particles are evaluated by a combination of in situ ^{13}C SP, surface-sensitive $^1H-^{13}C$ CP MAS NMR, and quantum chemistry calculations. The following results are obtained: At 180 °C, neat G2 decomposes on MgO to form surface-adsorbed $-OCH_3$ groups that are captured as a distinctive peak located at about 50 ppm in the CP/MAS spectrum. At low $Mg(TFSI)_2$ salt concentrations (i.e., 0.1 M $Mg(TFSI)_2$ in G2), the main solvation structure in this electrolytes is solvent-separated ion pairs, without extensive Mg−TFSI contact ion pairs. G2, likely including a small amount of G2-solvated Mg^{2+}, adsorbs onto the MgO surface. At high $Mg(TFSI)_2$ salt concentration (1.0 M $Mg(TFSI)_2$ in G2), contact ion pairs between Mg and TFSI are formed extensively in the solution with the first solvation shell containing one pair of Mg−TFSI and two G2 molecules and the second solvation shell containing up to six G2 molecules, namely, $MgTFSI(G2)_2(G2)_6^+$. In the presence of MgO, $MgTFSI(G2)_2(G2)_6^+$ adsorbs onto the MgO surface. Upon increasing the temperature to 180 °C, the MgO surface stimulates a desolvation process converting $MgTFSI(G2)_2(G2)_6^+$ to $MgTFSI(G2)_2^+$, releasing G2 molecules from the second solvation shell of the $MgTFSI(G2)_2(G2)_6^+$ cluster into the solution. The $MgTFSI(G2)_2^+$ and $MgTFSI(G2)_2(G2)_6^+$ tightly adsorb onto the MgO surface and are observed by $^1H-^{13}C$ CP/MAS experiments. The results contained herein show that electrolyte composition has a directing role in the species present on the electrode

DOI: 10.1021/acsami.9b11888
ACS Appl. Mater. Interfaces 2019, 11, 38689−38696

surface, which has implications on the structures and constituents of the solid−electrolyte interface on working electrodes and can be used to better understand its formation and the failure modes of batteries.

■ ASSOCIATED CONTENT

Supporting Information

The Supporting Information is available free of charge on the ACS Publications website at DOI: 10.1021/acsami.9b11888.

Spectral deconvolution for SP/MAS NMR and optimized geometry coordinates (PDF)

■ AUTHOR INFORMATION

Corresponding Authors

*E-mail: Jianzhi.Hu@pnnl.gov. Phone: (509) 371-6544 (J.Z.H.).

*E-mail: Karl.Mueller@pnnl.gov. Phone: (509) 371-6550 (K.T.M.).

ORCID

Jian Zhi Hu: 0000-0001-8879-747X

Nicholas R. Jaegers: 0000-0002-9930-7672

Ying Chen: 0000-0001-7417-0991

Kee Sung Han: 0000-0002-3535-1818

Hui Wang: 0000-0003-1997-2312

Vijayakumar Murugesan: 0000-0001-6149-1702

Karl T. Mueller: 0000-0001-9609-9516

Author Contributions

‡J.Z.H. and N.R.J. contributed equally.

Notes

The authors declare no competing financial interest.

■ ACKNOWLEDGMENTS

This work was supported by the Joint Center for Energy Storage Research (JCESR), an Energy Innovation Hub funded by the U.S. Department of Energy, Office of Science, Office of Basic Energy Sciences (BES). Experiments were conducted in the Environmental Molecular Sciences Laboratory (EMSL), a national scientific user facility sponsored by the Department of Energy's Office of Biological and Environmental Research at Pacific Northwest National Laboratory (PNNL). EMSL's supercomputers were utilized as a resource for computational modeling. PNNL is a multiprogram national laboratory operated for the DOE by Battelle Memorial Institute under Contract DE-AC06-76RLO 1830.

■ REFERENCES

(1) Lu, D.; Shao, Y. Y.; Lozano, T.; Bennett, W. D.; Graff, G. L.; Polzin, B.; Zhang, J. G.; Engelhard, M. H.; Saenz, N. T.; Henderson, W. A.; Bhattacharya, P.; Liu, J.; Xiao, J. Failure Mechanism for Fast-Charged Lithium Metal Batteries with Liquid Electrolytes. *Adv. Energy Mater.* **2015**, *5*, 1400993.

(2) Winter, M.; Brodd, R. J. What are Batteries, Fuel Cells, and Supercapacitors? *Chem. Rev.* **2004**, *104*, 4245−4270.

(3) Saha, P.; Datta, M. K.; Velikokhatnyi, O. I.; Manivannan, A.; Alman, D.; Kumta, P. N. Rechargeable Magnesium Battery: Current Status and Key Challenges for the Future. *Prog. Mater. Sci.* **2014**, *66*, 1−86.

(4) Hu, J. Z.; Rajput, N. N.; Wan, C.; Shao, Y.; Deng, X.; Jaegers, N. R.; Hu, M.; Chen, Y.; Shin, Y.; Monk, J.; Chen, Z.; Qin, Z.; Mueller, K. T.; Liu, J.; Persson, K. A. 25Mg NMR and Computational Modeling Studies of the Solvation Structures and Molecular Dynamics in Magnesium Based Liquid Electrolytes. *Nano Energy* **2018**, *46*, 436−446.

(5) Ding, M. S.; Diemant, T.; Behm, R. J.; Passerini, S.; Giffin, G. A. Dendrite Growth in Mg Metal Cells Containing Mg(TFSI)2/Glyme Electrolytes. *J. Electrochem. Soc.* **2018**, *165*, A1983−A1990.

(6) Ma, Z.; MacFarlane, D. R.; Kar, M. Mg Cathode Materials and Electrolytes for Rechargeable Mg Batteries: A Review. *Batteries Supercaps* **2019**, *2*, 115−127.

(7) Elvira, G.-B.; Francisco, G.-C.; Víctor, S.-M.; Alberto, M.-L. R. MgO-Based Adsorbents for CO2 Adsorption: Influence of Structural and Textural properties on the CO2 Adsorption Performance. *J. Environ. Sci.* **2017**, *57*, 418−428.

(8) Hu, M. Y.; Deng, X.; Thanthiriwatte, K. S.; Jackson, V. E.; Wan, C.; Qafoku, O.; Dixon, D. A.; Felmy, A. R.; Rosso, K. M.; Hu, J. Z. In Situ Natural Abundance 17O and 25Mg NMR Investigation of Aqueous Mg(OH)2 Dissolution in the Presence of Supercritical CO2. *Environ. Sci. Technol.* **2016**, *50*, 12373−12384.

(9) Ushikubo, T.; Hattori, H.; Tanabe, K. High Catalytic Activities of Specially Treated Mgo and Na Mgo for Decomposition of Methyl Formate. *Chem. Lett.* **1984**, *13*, 649−652.

(10) Parrott, S. L.; Rogers, J. W.; White, J. M. The decomposition of ethanol, propanol and acetic acid chemisorbed on magnesium oxide. *Appl. Surf. Sci.* **1978**, *1*, 443−454.

(11) Liang, S.; Gay, I. D. A C-13 Solid-State NMR-Study of the Chemisorption and Decomposition of Ethanol on MgO. *J. Catal.* **1986**, *101*, 293−300.

(12) Foyt, D.; White, J. M. Thermal-Decomposition of Methanol Adsorbed on Magnesia. *J. Catal.* **1977**, *47*, 260−268.

(13) Lowe, J. S.; Siegel, D. J. Reaction Pathways for Solvent Decomposition on Magnesium Anodes. *J. Phys. Chem. C* **2018**, *122*, 10714−10724.

(14) Shterenberg, I.; Salama, M.; Gofer, Y.; Levi, E.; Aurbach, D. The Challenge of Developing Rechargeable Magnesium Batteries. *MRS Bull.* **2014**, *39*, 453−460.

(15) Pals, C. R.; Newman, J. Thermal Modeling of the Lithium/Polymer Battery. *J. Electrochem. Soc.* **1995**, *142*, 3274−3281.

(16) Pals, C. R.; Newman, J. Thermal Modeling of the Lithium/Polymer Battery. *J. Electrochem. Soc.* **1995**, *142*, 3282−3288.

(17) Mahamud, R.; Park, C. Reciprocating Air Flow for Li-ion Battery Thermal Management to Improve Temperature Uniformity. *J. Power Sources* **2011**, *196*, 5685−5696.

(18) Jaegers, N. R.; Hu, M. Y.; Hoyt, D. W.; Wang, Y.; Hu, J. Z. Development and Application of In Situ High-Temperature, High-Pressure Magic Angle Spinning NMR. In *Modern Magnetic Resonance*; Webb, G. A., Ed.; Springer International Publishing: Cham, 2017; pp 1−19.

(19) Hu, J. Z.; Jaegers, N. R.; Hu, M. Y.; Mueller, K. T. In situ and ex situ NMR for Battery Research. *J. Phys.: Condens. Matter* **2018**, *30*, 463001.

(20) Deng, X.; Hu, M. Y.; Wei, X.; Wang, W.; Chen, Z.; Liu, J.; Hu, J. Z. Natural Abundance 17 O Nuclear Magnetic Resonance and Computational Modeling Studies of Lithium Based Liquid Electrolytes. *J. Power Sources* **2015**, *285*, 146−155.

(21) Baerends, E. J. A.; Berger, J. A.; Bérces, A.; Bickelhaupt, F. M.; Bo, C.; de Boeij, P. L.; Boerrigter, P. M.; Cavallo, L.; Chong, D. P. *Amsterdam Density Functional*. Theoretical Chemistry, Scientific Computing & Modelling (SCM), Theoretical Chemistry; Vrije Universiteit: Amsterdam, The Netherlands. (URL: http://www.scm.com).

(22) Grimme, S.; Ehrlich, S.; Goerigk, L. Effect of the Damping Function in Dispersion Corrected Density Functional Theory. *J. Comput. Chem.* **2011**, *32*, 1456−1465.

(23) Becke, A. D. Density-Functional Exchange-Energy Approximation with Correct Asymptotic Behavior. *Phys. Rev. A* **1988**, *38*, 3098−3100.

(24) Lee, C.; Yang, W.; Parr, R. G. Development of the Colle-Salvetti correlation-energy formula into a functional of the electron density. *Phys. Rev. B: Condens. Matter Mater. Phys.* **1988**, *37*, 785−789.

(25) Van Lenthe, E.; Baerends, E. J. Optimized Slater-Type Basis Sets for the Elements 1-118. *J. Comput. Chem.* **2003**, *24*, 1142−1156.
(26) Gottlieb, H. E.; Kotlyar, V.; Nudelman, A. NMR Chemical Shifts of Common Laboratory Solvents as Trace Impurities. *J. Org. Chem.* **1997**, *62*, 7512−7515.
(27) Hoyt, D. W.; Turcu, R. V. F.; Sears, J. A.; Rosso, K. M.; Burton, S. D.; Felmy, A. R.; Hu, J. Z. High-pressure Magic Angle Spinning Nuclear Magnetic Resonance. *J. Magn. Reson.* **2011**, *212*, 378−385.
(28) Turcu, R. V. F.; Hoyt, D. W.; Rosso, K. M.; Sears, J. A.; Loring, J. S.; Felmy, A. R.; Hu, J. Z. Rotor Design for High Pressure Magic Angle Spinning Nuclear Magnetic Resonance. *J. Magn. Reson.* **2013**, *226*, 64−69.
(29) Liang, S. H.; Gay, I. D. Adsorption and thermal decomposition of methanol on magnesium oxide. Carbon-13 NMR studies. *Langmuir* **1985**, *1*, 593−599.

DOI: 10.1021/acsami.9b11888
ACS Appl. Mater. Interfaces 2019, 11, 38689−38696